

Precipitation Extremes: Trends and Relationships with Average Precipitation and Precipitable Water in the Contiguous United States

KENNETH E. KUNKEL,^a THOMAS R. KARL,^b MICHAEL F. SQUIRES,^c XUNGANG YIN,^d
STEVE T. STEGALL,^a AND DAVID R. EASTERLING^c

^a *North Carolina Institute for Climate Studies, North Carolina State University, Asheville, North Carolina*

^b *Climate and Weather, LLC, Mills River, North Carolina*

^c *NOAA/National Centers for Environmental Information, Asheville, North Carolina*

^d *Riverside Technology, Inc., Asheville, North Carolina*

(Manuscript received 8 August 2019, in final form 8 November 2019)

ABSTRACT


Trends of extreme precipitation (EP) using various combinations of average return intervals (ARIs) of 1, 2, 5, 10, and 20 years with durations of 1, 2, 5, 10, 20, and 30 days were calculated regionally across the contiguous United States. Changes in the sign of the trend of EP vary by region as well as by ARI and duration, despite the statistically significant upward trends for all combinations of EP thresholds when area averaged across the contiguous United States. Spatially, there is a pronounced east-to-west gradient in the trends of the EP with strong upward trends east of the Rocky Mountains. In general, upward trends are larger and more significant for longer ARIs, but the contribution to the trend in total seasonal and annual precipitation is significantly larger for shorter ARIs because they occur more frequently. Across much of the contiguous United States, upward trends of warm-season EP are substantially larger than those for the cold season and have a substantially greater effect on the annual trend in total precipitation. This result occurs even in areas where the total precipitation is nearly evenly divided between the cold and warm seasons. When compared with short-duration events, long-duration events—for example, 30 days—contribute the most to annual trends. Coincident statistically significant upward trends of EP and precipitable water (PW) occur in many regions, especially during the warm season. Increases in PW are likely to be one of several factors responsible for the increase in EP (and average total precipitation) observed in many areas across the contiguous United States.

1. Introduction

Extreme precipitation events have played a major role in many national catastrophes and continue to be a chronic problem. They have been a driving factor in major socioeconomic losses including property damage and loss of life. For example, NOAA (2017) reports that since 1980 more than 1 trillion dollars in insured and uninsured property losses occurred from U.S. disasters with roughly 75% arising from flooding, tropical cyclones, and severe local storms, all of which are accompanied by extremes of precipitation (NOAA 2017). The American Society of Civil Engineers (2016) estimates that trillions of dollars will be needed by 2025 to

replace aging infrastructure in the United States, and of particular interest will be the design standards that are most appropriate. Loss of life has also accompanied excessive precipitation as floods resulted in over 4500 deaths in the United States between 1959 and 2005 (Ashley and Ashley 2008). Furthermore, extreme precipitation is associated with soil erosion and related environmental and ecological damages from soil degradation and water pollution (Soil and Water Conservation Society 2003). There is no doubt that extreme precipitation can be costly in terms of human safety and welfare, damages to housing and infrastructure, and environmental and ecological degradation.

Extreme precipitation-induced flooding spans across various time durations, from short-duration subdaily events to longer multiweek duration extreme precipitation totals. For example, the flood of 1993 was one of the worst disasters ever experienced in the central United States with an estimated \$18 billion in damages to

 Denotes content that is immediately available upon publication as open access.

Corresponding author: Kenneth E. Kunkel, kekunkel@ncsu.edu

property, agriculture, transportation, and other sectors. A single sector, the U.S. railroad industry, suffered physical damages amounting to \$282 million (2005 dollars) and lost revenues of \$198 million (Changnon 2006). The 1993 event was associated with a prolonged multimonth period of excessive precipitation in the central United States. Other events have been of much shorter duration, like the recent notable flood that affected the southeast United States in October 2016 from Hurricane Matthew's rainfall. The historic Houston, Texas, flooding associated with Hurricane Harvey in 2017 produced 2- and 3-day precipitation totals of 750 mm or more and weekly totals in excess of 1000 mm (Kunkel and Champion 2019). Sub-daily extreme precipitation events, often manifesting as flash-flood events, can also lead to catastrophic impacts and loss of life.

Given the practical significance of these extreme precipitation events, it is not surprising that the scientific, engineering, and planning communities across the United States have devoted considerable attention assessing whether these events are changing in frequency and intensity (Melillo et al. 2014; Wuebbles et al. 2017). These assessments have in part relied on a number of studies of U.S. precipitation that have found an upward trend in heavy events (Karl and Knight 1998; Groisman et al. 2005; Walsh et al. 2014). On the basis of one particular extremes metric (2-day precipitation totals exceeding a threshold for an average recurrence interval of 1 in 5 years), the greatest increases have been in the upper Great Plains, Midwest, and Northeast where increases are 30% above the 1901–60 average (Walsh et al. 2014). Coincidentally, there have been more flooding events in the Midwest and Northeast where the largest increases in extreme rainfall have occurred (Melillo et al. 2014). In many areas of the world heavy rainfall events are becoming more intense and more frequent and the amount of rainfall in extreme events has been increasing (IPCC 2013). Considering the effects of a warmer world, increased urbanization, continued development in floodplains and coastal areas, and land-use changes, the risks of increased future floods are significant (Doocy et al. 2013).

Typically, studies of the trends in extreme precipitation trends have used a single definition, or just a few metrics for extreme precipitation. Quantitative comparison across studies is difficult or infeasible because of the differences in definitions. Kunkel and Frankson (2015) examined trends in four different metrics of extreme precipitation and generally found upward trends over the United States in all of the metrics, but they did not quantify the trends. Surprisingly, no studies have documented regional changes of precipitation extremes in the United States across a wide range of durations and

return intervals. Karl and Knight (1998) did show that about one-half of the total daily precipitation in the United States falls in the upper 10th percentile of precipitation events and that these events are increasing, but what this looks like in rarer precipitation events, seasonally and regionally, remains to be explored. So, for this analysis, the magnitude of the trends of regionally averaged extreme precipitation events is explored for various average return intervals (ARIs) and durations throughout the year as well as for the warm (May–October) and cold seasons (November–April). This also includes the contribution to the trend of average precipitation P .

Most important is that confidence in future changes in extreme precipitation frequency and intensity is dependent on understanding the driving factors of observed increases. Integrated column atmospheric water vapor, that is, precipitable water (PW), is known to be an important consideration in probable maximum precipitation computations (Kunkel et al. 2013). It has yet to be demonstrated, however, that observed trends in extreme precipitation events (EP) are related to trends in PW. In this analysis the regional trends of extreme precipitation are evaluated for a variety of ARIs and durations for the warm and cold seasons as related to trends in PW and P .

2. Data and method

a. Precipitation

Daily precipitation values were obtained from the Global Historical Climate Network—Daily (GHCN-D; Menne et al. 2012). GHCN-D undergoes a rigorous and robust quality control process (Durre et al. 2008, 2010) that results in suspicious data being flagged for various errors. If a daily precipitation value fails any of the 14 automated quality checks except for the “duplicate check,” it is not used. The duplicate check looks for the duplication of sequences of data in different time periods. For example, two different months in the same year having identical values. These types of problems usually occur because of keying, transmission, or processing errors (Kunkel et al. 1998). Observations that failed the duplicate check were investigated, and the correct series of values were used and the truly duplicate series of values were not used.

To ensure a uniform analysis across the contiguous United States and to ensure robust results, rather stringent missing data criteria were applied to select stations for analysis. The period of analysis is 1949–2016, which encompasses the time period of recent extreme-event increases documented in other studies (e.g., Walsh et al. 2014). Specifically, stations used in

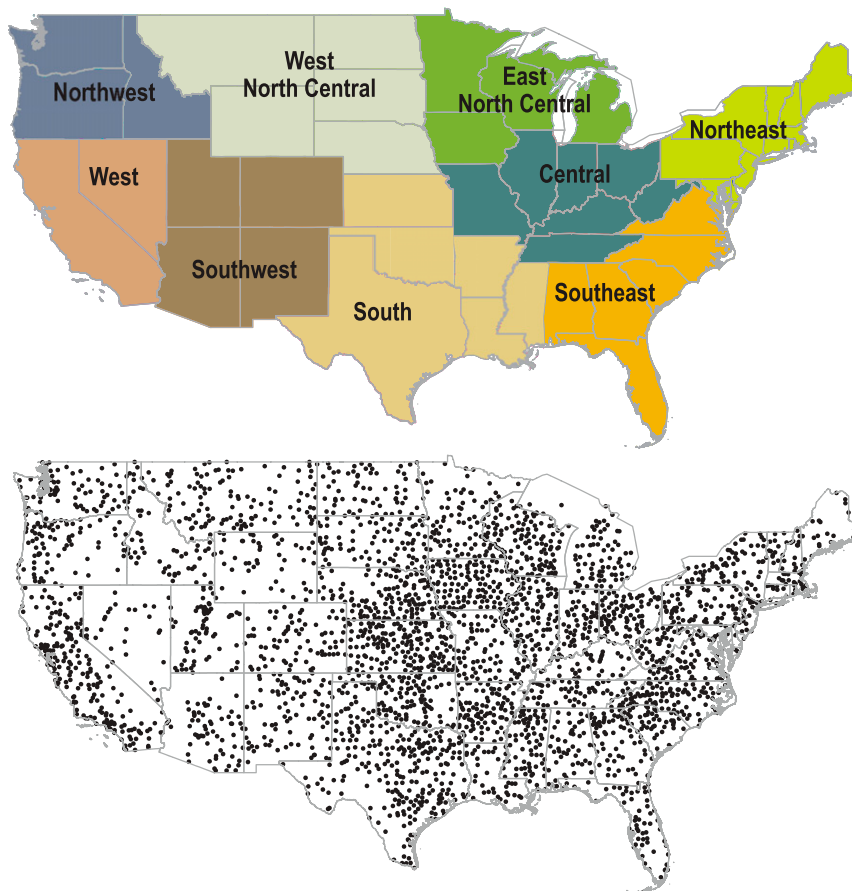


FIG. 1. (top) The National Centers for Environmental Information climate regions, and (bottom) the 3098 stations used for extreme-value statistics that passed quality and completeness criteria. See the text for details. Abbreviations for the regional titles are Northwest—NW, West North Central—WNC, East North Central—ENC, Northeast—NE, West—W, Southwest—SW, South—S, Central—C, and Southeast—SE.

the analysis had to be at least 90% complete (less than 10% missing daily values) during the 1949–2016 period. Once stations were selected based on this criterion, another criterion was applied in regional aggregations of the station analyses. For a station to be included in the annual value of a regional time series for a particular year, the station had to have at least 300 days with valid precipitation data for any given year. One last criterion was applied to specific events: an event for a particular duration could have no more than 10% missing days. Thus, for durations less than 10 days, no missing data were allowed. These completeness criteria are identical to those used by [Kunkel and Frankson \(2015\)](#) in their study of global precipitation extremes. The spatial distribution of the 3098 stations that passed quality and completeness checks is shown in [Fig. 1](#) (bottom panel). Spatial coverage is very good across most of the United States. A few areas in the western mountainous United States have notably sparser coverage,

such as Nevada, Idaho, Utah, Wyoming, northern Arizona, and eastern Oregon. The use of a broader regional aggregation process helps overcome coverage deficiencies in the western mountains. The inclusion of regional extreme precipitation for Alaska and Hawaii was not feasible, given the complex terrain and sparsity of stations in those states.

The choices of duration and rarity of extreme precipitation events used for this analysis relate to an important subset of needs for design of infrastructure that are used by the civil engineering community and others. Specifically, the rarity is defined in terms of the frequency via the ARI or sometimes called “return period” (or expressed as the “annual exceedance probability,” that is, the inverse of ARI), with ARI values of 1, 2, 5, 10, and 20 years being analyzed. Larger values of ARI are often used in design, but at these ARI values, such as 100 years, sampling uncertainty (noise) makes it difficult to demonstrate robust trends. Durations were calculated

for 1, 2, 3, 5, 10, 20, and 30 days. Therefore, in this analysis 35 combinations of duration and frequency were used. Daily observations of precipitation are used to maximize the spatial density of stations at the expense of exploring subdaily extremes. Subdaily precipitation rates are also of great interest, including the civil engineering community, but at this time the spatial density of stations with sufficient period of records do not lend themselves to robust calculation of regional average trends of rare events. Additionally, compared to the GHCN-derived daily precipitation data, other subdaily gauge datasets [e.g., the National Centers for Environmental Information (NCEI) Hourly Precipitation dataset] have not had the same level of quality assessments.

Regional aggregated analyses were defined by the climate regions used by NCEI. The nine NCEI climate regions (Fig. 1, top panel) are used to summarize many NCEI products and were originally defined by monthly mean surface moisture anomalies using the Palmer drought severity index (Karl and Koscielny 1982; Karl and Koss 1984) so the regions are strongly tied to precipitation. Trends and significance were estimated for each of the 35 combinations within each region. Given the large interannual variability and nonnormality of precipitation, especially heavy precipitation, we use the nonparametric Kendall's tau to test the trends for statistical significance (Hollander and Wolfe 1973) at the 0.05 level (0.025 in each tail).

The method to compute extreme-event trends is an empirical approach similar to that used in some recent studies (e.g., Kunkel and Frankson 2015; Walsh et al. 2014). An annual time series of extreme events was computed for each station using a peaks-over-threshold (POT) method (Wilks 2006). So, for a 5-day event with an ARI of 10 years, we would expect that value to occur seven times in our 68-yr record ($68/10 = 6.8$, which rounds to 7). Therefore, the seven highest 5-day precipitation events are identified in the time series. Note that for any given station most years will be zero, some years will have one event, and it is possible for some years to have multiple events, but the total number of 5-day events in the time series will be 7. Table 1 lists the expected number of occurrences for each ARI. To provide a measure of independence between events, a 2-day separation is required between the end of one event and the beginning of another. For example, if the highest 5-day, 10-yr ARI total is 7–11 July 1993, none of the other six events can end after 4 July or begin before 14 July 1993. This process is repeated for each duration/ARI combination to produce 35 annual occurrence time series for each station.

To reduce the relatively large interannual variability of point station measurements, a regionally aggregated

TABLE 1. Relationship between average recurrence interval and number of events to be identified during the 68-yr period spanning 1949–2016, along with the gridcell size used to aggregate to regions.

Avg return interval	Expected no. of occurrences in 68-yr period	Gridcell size
20	3	$6^\circ \times 6^\circ$
10	7	$6^\circ \times 6^\circ$
5	14	$4^\circ \times 4^\circ$
2	34	$2^\circ \times 2^\circ$
1	68	$2^\circ \times 2^\circ$

time series from the station time series was calculated. The goal was to produce a true area-averaged metric that does not overweight areas with higher-than-average station density or underweight areas with lower-than-average station density (Fig. 1, bottom panel). To address this, gridcell average time series are first produced from the station time series. The gridcell average time series is simply the arithmetic average of all stations within the grid cell. The size of the grid cell is a function of the ARI. Less-extreme events (1 and 2-yr ARIs) are averaged to $2^\circ \times 2^\circ$ grid cells. Events that are the most extreme (10- and 20-yr ARIs) are much less common and are therefore aggregated into $6^\circ \times 6^\circ$ grid cells to support robust trend and significance calculations at the gridcell scale (Table 1). These grid cells are then aggregated up to the regional (nine climate regions) and a national level. Given the 9 climate regions, 1 national aggregation, and 35 duration–ARI combinations, there are a total of 350 time series for extreme precipitation analysis and interpretation.

Since the precipitation data could potentially drop out in a nonrandom manner, a few checks were made to assess this possibility. Throughout the period of record, no fewer than 89% of the stations were available, with the lowest percentage occurring in 1949, a peak to 99% around 1960, and a slow decay to 89% again around 2010. This was sufficient to ensure that the number of grid cells with at least one station does not vary over time by more than 2%. Because the precipitation data were partitioned into the cold and warm seasons, checks were made to assess significant systematic differences in missing data between seasons. The percent of available station data during the warm and cold seasons remained within 1%–2% of each other throughout the period of record.

For each of the annual, the cold-season, and the warm-season periods, a trend and its statistical significance was calculated. For each time series, least squares linear regression is used to estimate the magnitude of the trends. Linear trends are used as gross estimate of the direction of change and are not meant to imply all the trends are linear. To help to protect against large interannual variability, nonnormality, and

nonlinearity of the time series conflating statistical significance, the nonparametric Kendall’s tau is used to test for significance (Hollander and Wolfe 1973). Trends were calculated for the full period of record and a subset period of 1979–2016.

In addition to the extreme-event trends, similar trends were calculated for total precipitation. The data were partitioned into seasons s , where s represents aggregation of the warm or cold season or annually. This enables assessment of the times of the year that contribute most strongly to both the annually and seasonally segregated POT extreme-event trends for each of the ARIs, durations, and regions. The percent contribution for a specific extreme metric to the trend of total precipitation (both extreme and nonextreme precipitation) is given by δ , where

$$\delta_{\text{ARI},d,s} = [T(\text{EP}_{\text{ARI},d,s})/T(P_s)] \times 100\%; \quad (1)$$

$T(\text{EP}_{\text{ARI},d,s})$ is the trend of the amount of extreme precipitation for a specific average return period, duration, and season (or seasonless time period), and $T(P_s)$ is simply the trend of the total precipitation for the warm or cold season or annually. Values of $\delta_{\text{ARI},d,s}$ are compared within and across regions. The magnitude of $\delta_{\text{ARI},d,s}$ reflects the degree of influence that extreme precipitation events had on the trend of total precipitation.

b. Water vapor

The National Centers for Environmental Prediction–National Center for Atmospheric Research (NCEP–NCAR) reanalysis (Kalnay et al. 1996) and NASA’s MERRA-2 reanalysis (Gelaro et al. 2017) were used to calculate trends (1979–2016 for NCEP–NCAR and 1980–2016 for MERRA-2) of PW. Because the NCEP–NCAR and MERRA-2 reanalyses have resolutions of $2.5^\circ \times 2.5^\circ$ and approximately $0.5^\circ \times 0.625^\circ$, respectively, these resolutions lend themselves to the methods of regional and gridcell averages used here for extreme precipitation. Wang and Zhang (2008) show standard errors and biases of radiosonde and GPS measurement of PW are about 1 mm. This is small relative to PW during extreme precipitation events, which are usually between about 10 and 75 mm.

Although the NCEP reanalysis is available prior to 1979, the homogeneity of the PW trends was paramount. The homogeneity of the water vapor trends during the time since 1979 is aided by at least three issues. First, since 1979 microwave satellite water vapor measurements have been assimilated into the reanalyses, but prior to this time they were not available. Use of longer records dating back to 1949 can lead to misleading inhomogeneities.

Second, the focus of this analysis is over the United States and Trenberth et al. (2005) has shown that the PW from the NCEP reanalysis are reasonable where they are constrained by radiosondes, unlike the sparser coverage over the open oceans and during the mid-twentieth century in the United States. Third, to ensure a measure of robustness of the PW trends, seasonal and annual comparisons of PW trends of the two reanalyses are used to help bound PW trend uncertainties and provide a central estimate.

Linear trends of the annual and seasonal averages of PW_s , $T(\text{PW}_s)$, were calculated across the contiguous United States, including all the regions and nationally. Seasonal and annual averages were calculated, as opposed to averaging the values of PW using only the dates of the events. This is because of the various 24-h precipitation accumulation times (1, 2, . . . , 30 days) used for the large set of stations in this analysis. Many of the stations used in this analysis are manually read by observers during the morning or early evening, making it difficult to be confident of the exact date of precipitation. As a result, this requires us to assume that the magnitude of $T(\text{PW}_s)$ is representative across the full distribution of PW—for example, that trends in the average are representative of trends in the upper end of the distribution. Although this is likely to be a good rough estimate, and we have no reason to believe otherwise; further research—for example—quantile trends, is warranted to test the impact of such an assumption.

Using the calculated values of $T(\text{PW}_s)$ and $T(\text{EP}_s)$, a correlation coefficient R was computed using the warm- and cold-season trends for each region (“reg”) and each reanalysis (“rea”). This resulted in 36 pairs (9 regions \times 2 seasons \times 2 reanalyses) of $T(\text{PW})$ and $T(\text{EP})$ that were cross correlated. The correlation R for each ARI–duration combination is given by

$$R_{\text{ARI},d} = \text{COV}_{T(\text{PW}_s,\text{reg,rea}),T(\text{EP}_s,\text{reg,rea})}/S_{T(\text{PW})}S_{T(\text{EP})}, \quad (2)$$

where $\text{COV}_{T(\text{PW}),T(\text{EP})}$ is the covariance of the trends and $S_{T(\text{PW})}$ and $S_{T(\text{EP})}$ are the standard deviation of the trends of $T(\text{PW})$ and $T(\text{EP})$, respectively. Given the expected positive correlation of the two trends, the statistical significance of the correlation of the trends was assessed at the 0.01 significance level for a one-tailed test using a t -test statistic.

3. Results and discussion

a. Total precipitation and trends

Figure 2 shows that there is considerable spatial variability in $T(P_s)$ and P_s . The annual amount of precipitation increases from the southwest to the northeast. The eastern

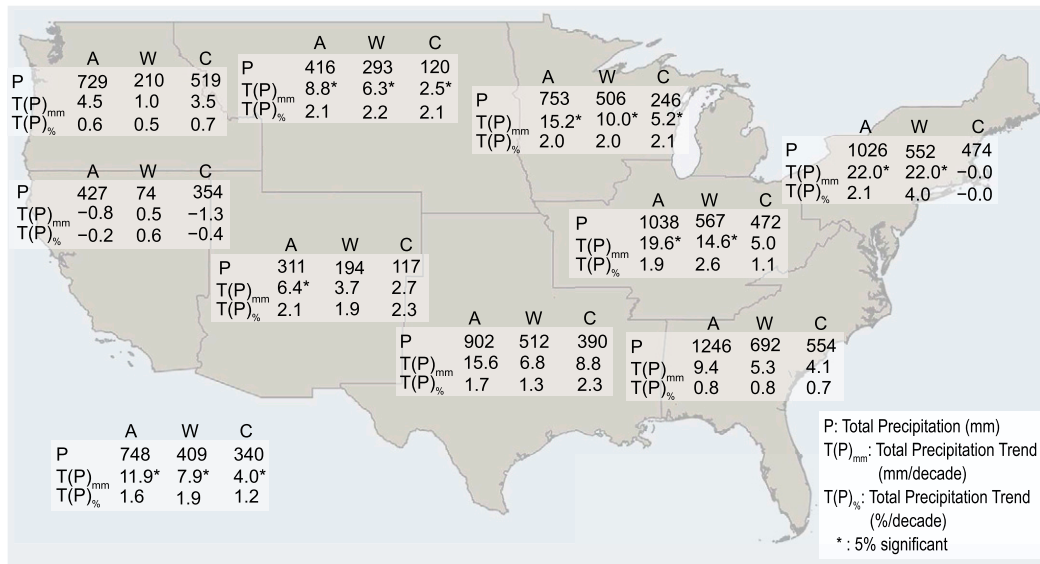


FIG. 2. Precipitation climatology statistics for the nine regions and the United States as a whole; P is the average precipitation without regard to season (label A for annual) and for the warm (label W) and cold (label C) seasons, $T(P)_{\text{mm}}$ is the linear trend [1949–2016; $\text{mm} (10 \text{ yr})^{-1}$], and $T(P)_{\%}$ is the trend in percent per decade of the total [$T(P)_{\text{mm}}/P$] $\times 100\%$. Statistically significant trends in a two-tailed test are noted by an asterisk.

regions of the nation (the NE, SE, C, and S; note that the abbreviations of all nine regions are explained in the caption of Fig. 1) are the wettest, with about 20% more precipitation occurring in the warm season than in the cold season. In contrast, most regions in the western half of the United States have less than one-half of the precipitation of the four wetter regions, with the NW and ENC regions falling between these extremes. Outside the four eastern regions there are strong seasonal cycles, with 2–3 times as much precipitation falling in the wet season. This occurs during the cold season for the NW and W regions and during the warm season for the SW, ENC, and WNC.

The largest and most significant positive values of $T(P_s)$ occur in the three most northerly regions (excluding the NW) and the C region, and this result is largely attributed to trends in the warm season. Seasonal decomposition of the trends of PW will provide insights regarding potential causes of the increase. With the exception of the W region, all other regions also have positive values of $T(P_s)$, but few are statistically significant even though the magnitude and percent of the positive trends in the SW, S, and SE are substantial.

b. Extreme precipitation trends for an example region

Figure 3 shows the T(EP) for the 35 duration–frequency combinations in the NW region. The 5-day, 10-yr ARI has a trend of -1% per decade and it is not statistically significant. The 1-day, 20-yr ARI is increasing at a rate of 8% per decade and is statistically significant in contrast

to the decreasing trend of -7% per decade for the 10-day duration. Thus the 1-day heavy precipitation events that typically occur once in a generation are occurring more frequently, while the 10-day duration events for the same recurrence interval are decreasing. Given the variability of the trends for the 20-yr recurrence interval, caution is needed when interpreting cell-to-cell variations for specific durations and ARIs. Rather, a more general assessment requires consideration of the broad patterns that emerge from the set of ARIs and durations. These broader patterns are much more likely to reveal signals with physical significance as compared with the noisier trends of that can arise for an individual region, duration, and ARI.

c. Annual trends of the extremes across the regions

The year-by-year annual time series of the 5-day, 10-yr ARI (Fig. 4) further illustrate the perils of emphasis on any single metric for extreme precipitation. The time series in Fig. 4 display considerable variability from year to year within each region and this can mask or imitate trends. The peril is less at the national level where the interannual variability is smaller due to spatial aggregation, but the practical use of this information at the national level of aggregation is less useful. In the analysis in this paper, with 350 precipitation metrics and 3 times that number with the annual and two seasons, the interpretation of the results will be heavily based on the preponderance of consistent trends within and among the tables.

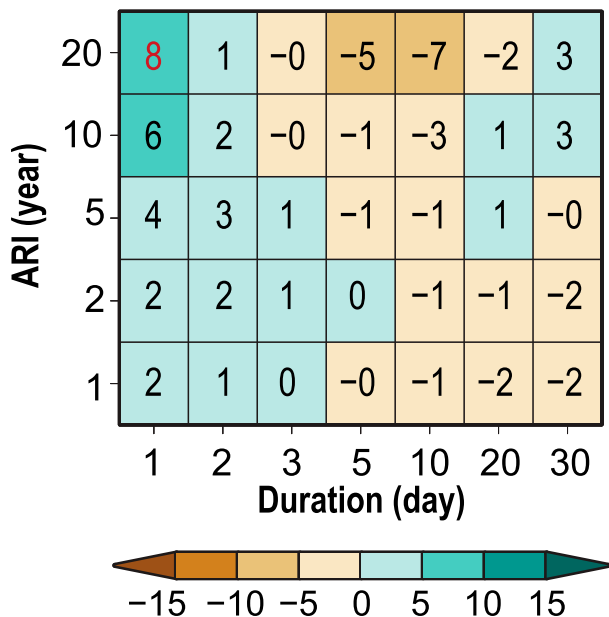


FIG. 3. Trends (percent per decade) in the frequency of occurrences for the NW region during the 1949–2016 period for the 35 duration–ARI combinations. Decreasing trends are displayed in shades of brown, and increasing trends are displayed in shades of green. Statistically significant trends are shown in red-colored numbers (0.05 significance level for a two-tailed test). See the text for details.

As depicted in Fig. 5a there are notable spatial and temporal patterns of $T(EP)$. A striking feature of the pattern in Fig. 5a is the gradient from west to east of the sign and magnitude of the trends. There are large positive trends in the six regions: NE, SE, S, C, ENC, and WNC where the NE and C regions have more than 30 of the 35 trends statistically significant. Positive trends of 5% to 15% per decade are common in these areas with some as high as 15% to 20% per decade in the NE. This is in contrast to the two westernmost regions, the NW and W, where mixed trends of extreme precipitation events are evident.

The magnitude and significance of the positive trends increase as the events become rarer (e.g., a 1-yr recurrence interval vs a 20-yr recurrence interval), as can be readily discerned in Fig. 5a by the deeper shades of green in the top rows versus the lower rows. This is most obvious in the national aggregate. This characteristic is ubiquitous across the United States. It is noteworthy that despite the widely different signs and magnitudes of the trends moving from west to east, the same tendency appears in all regions with the trends of rarer events being of greater magnitude and more statistically significant. This is suggestive of a nonlinear impact of changes in dynamics or thermodynamics affecting extreme precipitations events. Over the last several decades (since

1979), the trends in Fig. 5b reveal patterns that are very similar to the earlier start date of 1949 (Fig. 5a).

d. Trends of the extremes during the warm and cold seasons

In general, with the exception of the NW, W, and S regions, positive values of $T(EP_s)$ are substantially larger and best reflected during the warm season regardless of starting date when compared with the cold season (Figs. 6 and 7). Even for regions such as the NE and SE where the P_{cold} approaches that of P_{warm} (within 15%–20%, Fig. 2), the values of $T(EP_{warm})$ are substantially larger than the $T(EP_{cold})$. In the W and NW, both cold- and warm-season trends are mixed, albeit the magnitude is higher in the cold wet season. In the S, the warm- and cold-season $T(EP_{warm})$ and $T(EP_{cold})$ are not substantially different. Within each season the relative magnitude (in percent) of the $T(EP_s)$ tends to vary similarly to the magnitude and sign of $T(P_s)$. This is suggestive of a common factor, such as PW, affecting precipitation intensities from light to extreme.

e. Comparative analysis of the trends in extreme and total precipitation

For all regions with the exception of the NW and W, the relatively high values of δ means that $T(EP)$ is responsible for a significant proportion of $T(P)$ (Fig. 8). A distinguishing difference between δ and $T(EP)$ (Fig. 5) is the juxtaposition of the large values of the trends for the short versus the long ARIs. This is because the trends of the more frequent extreme precipitation events contribute much more to the total trend, despite the fact the trend in the number of occurrences of the events is less. Spatially, $T(EP)$ is an increasingly larger fraction of $T(P)$ moving west to east where $T(EP)$ is more significant. Another clear characteristic is the generally larger values of δ for longer durations and less rare events where over 50% of the total precipitation trend is often observed for the extreme metric of 30 days with an average recurrence interval of 1 year. This is attributable to the greater accumulation of precipitation at 30 days versus fewer days and the greater number of events. Arguably, however, what is most notable in Fig. 8 is the relatively large values of δ even for the short-duration events, for example, 1, 2, and 3 days with 1-yr recurrence interval. Here, about one-third of $T(P)$ is contributed by $T(EP)$. This means that these short-duration extreme events that occur on average every year have a disproportionately large influence on $T(P)$. This is ubiquitous for all regions [where $T(P)$ exceeds $1 \text{ mm} (10 \text{ yr})^{-1}$] including the NW where δ has mixed signs depending on the duration of the events. The importance of δ for the rarest event studied, 1 in 20 years, is still noteworthy where 5%–30% of $T(P)$

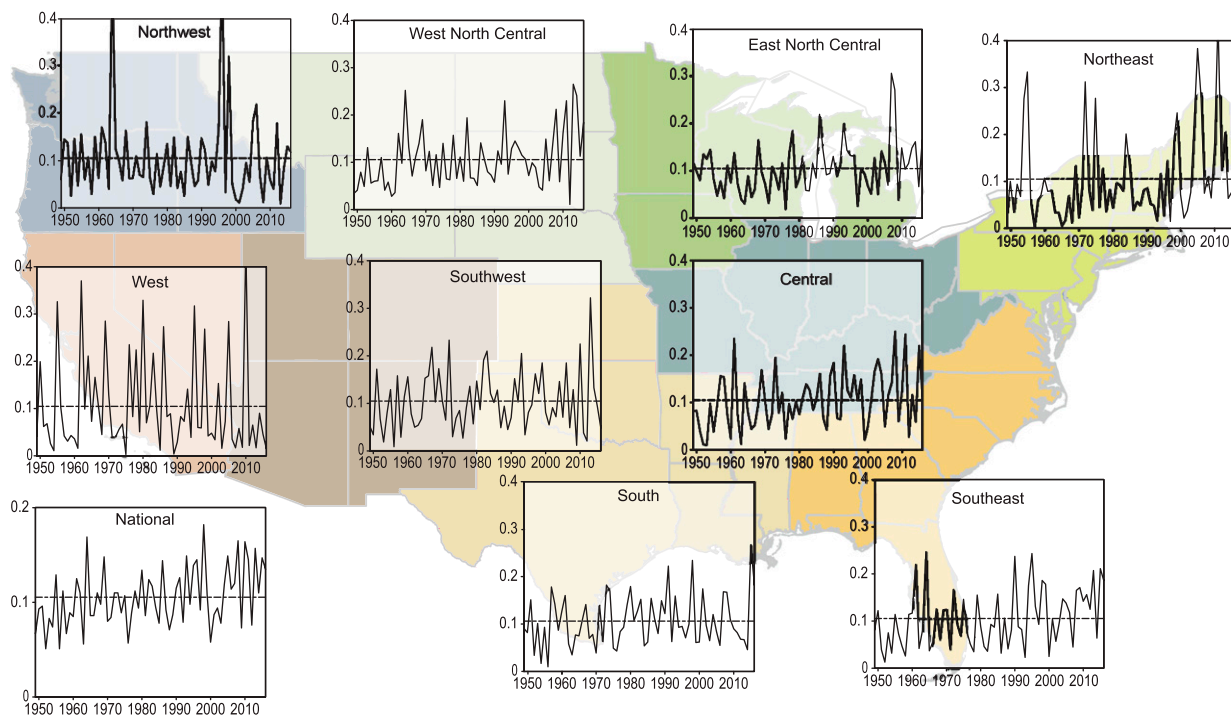


FIG. 4. Regional annual counts (peaks over threshold) time series for the combination of 5-day duration and 10-yr ARI averaged across the nine NCEI regions as well as the national time series. The units are number of events per station per year. The horizontal dashed line represents the long-term average.

is explained by $T(EP)$ for most regions. These results suggest that it is very important to understand the causes of the $T(EP)$ if $T(P)$ is to be fully explained. This would be consistent with the notion that $T(EP)$ is more sensitive to trends of other variable(s) when compared with events with less precipitation. Trends in PW is a candidate.

The seasonal decomposition of the seasonless results for δ is very different for the warm (Figs. 9a,b) versus the cold seasons (Figs. 10a,b). The larger contribution of $T(EP_s)$ toward $T(P_{\text{Annual}})$ in the warm season versus the cold season is clearly evident in these two figures. The magnitude of δ and the greater frequency of its statistical significance in the warm season reflects this characteristic. Nationally, even though the average precipitation in the warm season is only 20% higher than the cold season and the value of $T(P_{\text{warm}})$ is about 2 times that of $T(P_{\text{cold}})$, the values of δ are often 5–10 times as large. With few exceptions, the warm-season extremes are disproportionate in their influence on $T(P)$ relative to the cold season in all regions depicted in Figs. 9 and 10.

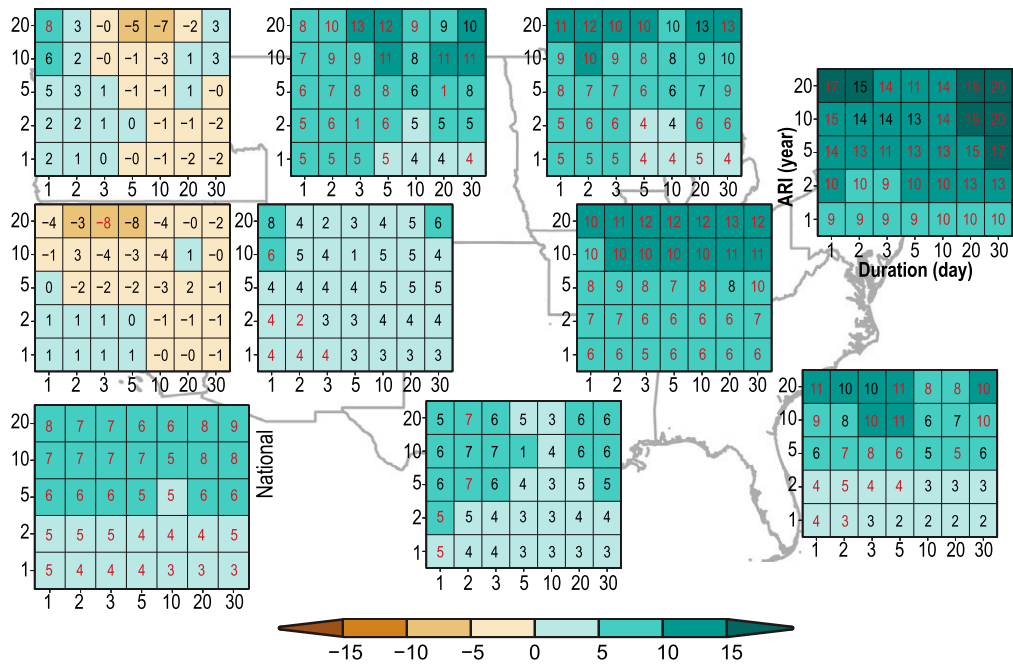
A comparison of Figs. 9b and 10b where the numerator and denominator of δ take on the same season shows some remarkably large values of δ . For example, in the SE during the warm season large values of δ are found for all event durations and rarity, ranging from a minimum of 22% to a maximum of 98% of $T(P_{\text{warm}})$ accounted for

by $T(EP_{\text{warm}})$. Substantially smaller and less significant δ values are generally found in the cold season. Larger values of δ during the warm versus the cold season are reflected in the frequent occurrence of values of δ exceeding 50% during the warm season and virtually absent during the cold season. Although much less influential on $T(P_{\text{cold}})$ relative to the warm season, on a national scale $T(EP_{\text{cold}})$ still plays a substantial role on the positive values of $T(P_{\text{cold}})$ as depicted by about one-third of the values of δ_{cold} exceeding 15%.

f. Assessing the similarity of extreme precipitation to water vapor trends

Weather and climate model studies have identified a variety of potential factors that influence model-generated extreme precipitation rates, and water vapor has been shown to be a key contributor (Nie et al. 2018; O’Gorman and Schneider 2009; Kitoh and Endo 2016; Bao et al. 2017; Thackeray et al. 2018; Giorgi et al. 2019). Kunkel et al. (2013) have presented the case for the design storm dependencies on large amounts of water vapor as a key forcing factor for extreme precipitation events, and water vapor is expected to increase substantially as the climate warms (IPCC 2013). Seager et al. (2015) have already shown that, over the period 1960–2013, the observed surface water vapor pressure

(a) Annual Trend (% per decade), 1949–2016



(b) Annual Trend (% per decade), 1979–2016

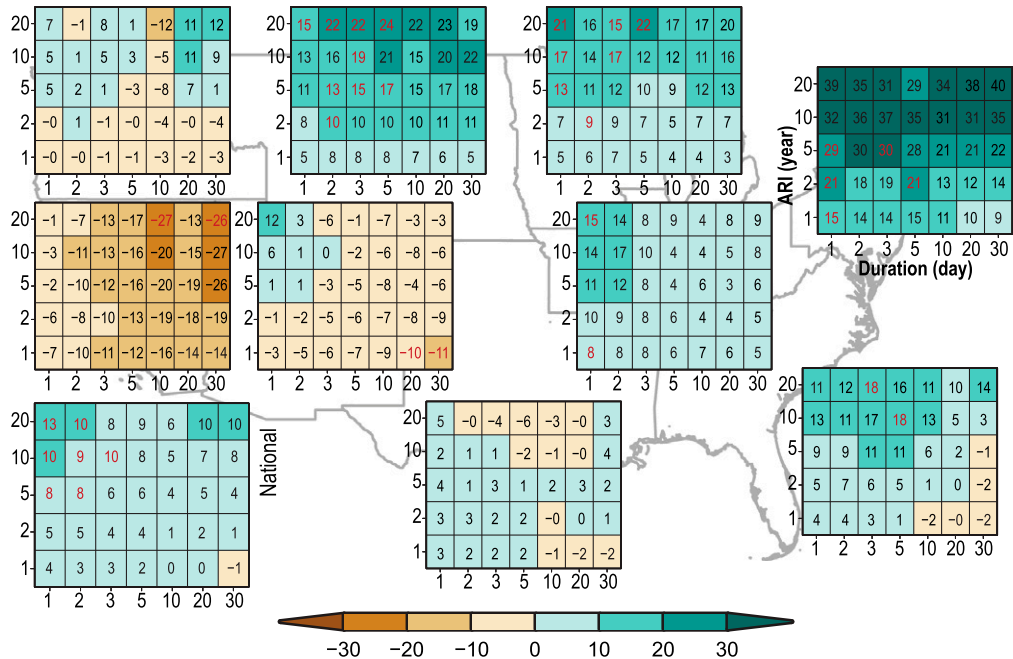
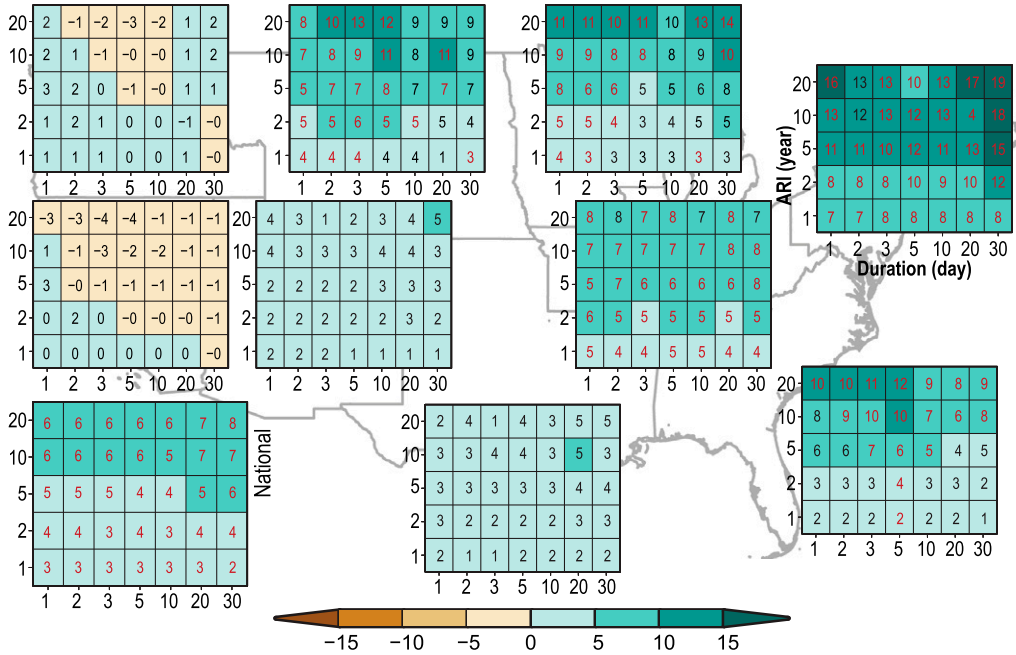


FIG. 5. As in Fig. 3 (annual trend), but for each of the nine NCEI regions as well as a national aggregation (shown in the lower left of each panel) for (a) 1949–2016 and (b) 1979–2016.

(a) Warm Season Trend (% per decade), 1949–2016



(b) Warm Season Trend (% per decade), 1979–2016

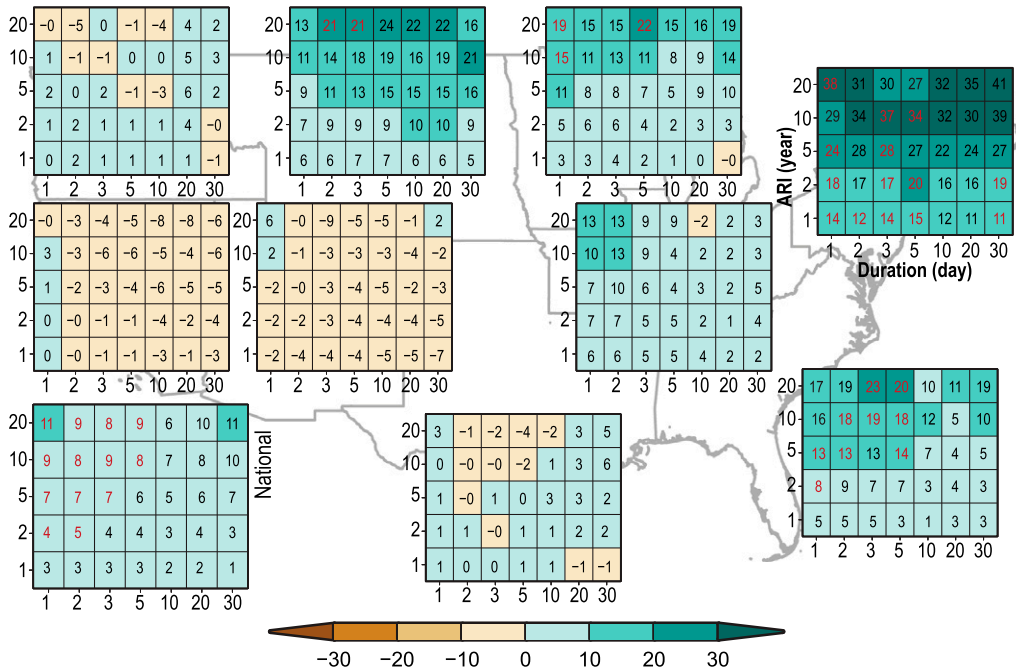
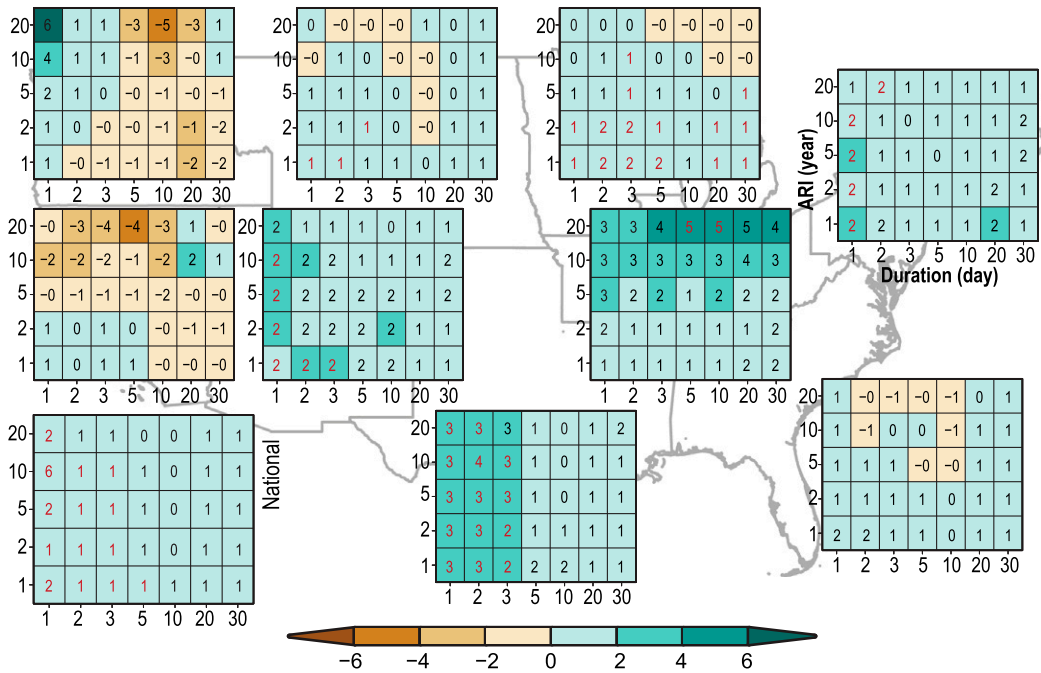


FIG. 6. As in Fig. 5, but for warm-season (May–October) trends.

(a) Cold Season Trend (% per decade), 1949–2016



(b) Cold Season Trend (% per decade), 1979–2016

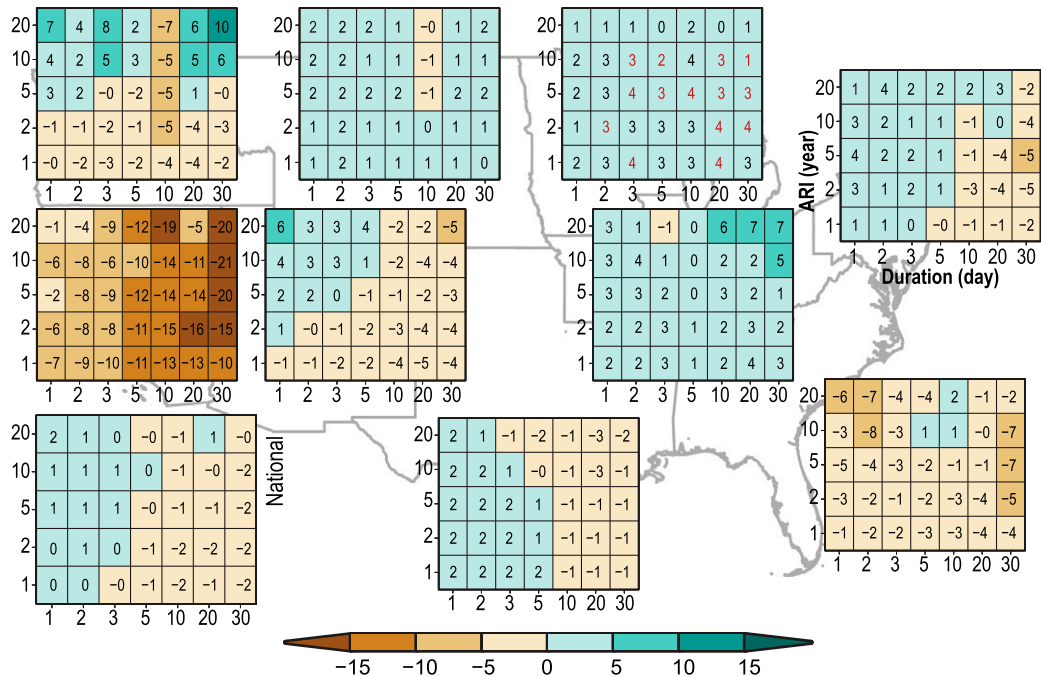


FIG. 7. As in Fig. 5, but for cold-season (November–April) trends.

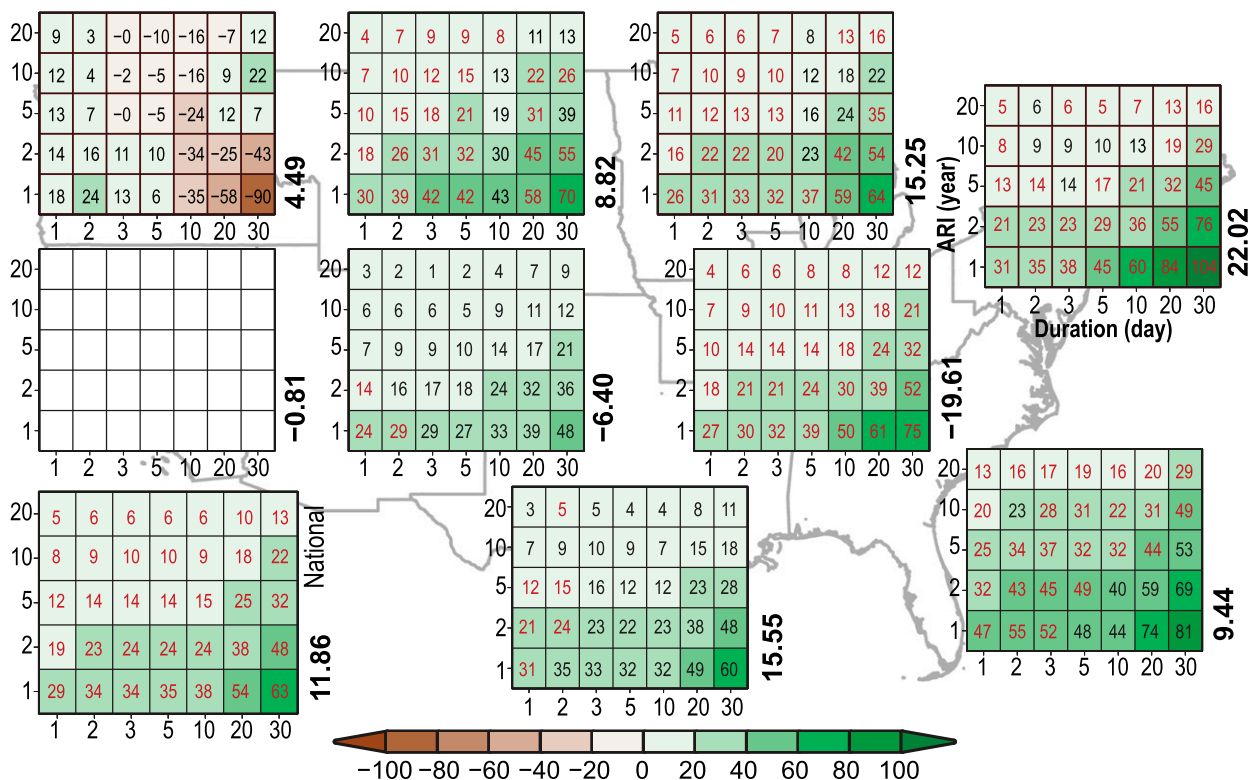


FIG. 8. Values of $\delta_{ARI,d,annual}$, with red denoting statistical significance of $T(EP)$ at the 0.05 level. The rotated numbers to the right of each table are annual values of $T(P)$ [$\text{mm} (10 \text{ yr})^{-1}$]. The West regional table is blank because $T(P_{annual})$ is near zero.

is increasing in many areas of the United States and is increasing more during the warm season than during the cold season in much of the northeastern two-thirds of the United States. This section focuses on the relationship between the trends of total column water vapor (PW) with the frequency of extreme events for the ARIs and durations used in this study during the period 1979–2016 in context with previous work related to trends in weather events associated with extreme precipitation.

Figure 11 reveals considerable agreement in $T(PW)$ between NCEP–NCAR and MERRA-2. Both reanalyses generally show upward trends of $T(PW)$, although MERRA-2 shows stronger and more spatially uniform trends. This is most evident during the warm season (Fig. 11c vs Fig. 11d) when the upward trends of $T(EP)$ are highest. Both reanalyses show decreases of $T(PW)$ in the SW during the cold season, but NCEP–NCAR also has downward values of $T(PW)$ along the East Coast in contrast with upward trends in MERRA-2. The downward trends of NCEP–NCAR during the cold season are more consistent with the mixed and downward values of $T(EP)$ in the NE and SE, respectively. Nonetheless, on this basis alone it is not possible to assess which reanalysis better represents $T(PW)$.

Across the nine regions, $T(PW)$ and $T(EP)$ are positively correlated across all ARIs and durations as shown in Table 2. As expected, all of the correlations are positive and are also statistically significant at the 0.01 level. This clearly indicates that PW is a key factor in explaining the $T(EP)$. In addition, there is discernable pattern in the magnitude of the correlations. They are higher across all ARIs for short-duration events and lower across all the ARIs for long-duration events, for example, 1 day versus 30 days. This is opposite to what might have been expected because $T(PW)$ represents the seasonal average as opposed to the trend during the events. This suggests that there are other factors affecting $T(EP)$ that are time-duration sensitive. We postulate that the persistence of large-scale circulation patterns and synoptic weather events is increasingly important as duration time increases and that feedback effects of water vapor such as vertical velocity and latent heat of condensation are disproportionately important for short-duration extreme precipitation events.

The work of Kunkel et al. (2012) provides a basis for further investigation of the causes of the decrease in R as the durations increase as well as helping to explain the unexplained variance in the relationships between $T(PW)$ with $T(EP)$ across the regions. Kunkel et al. (2012) show

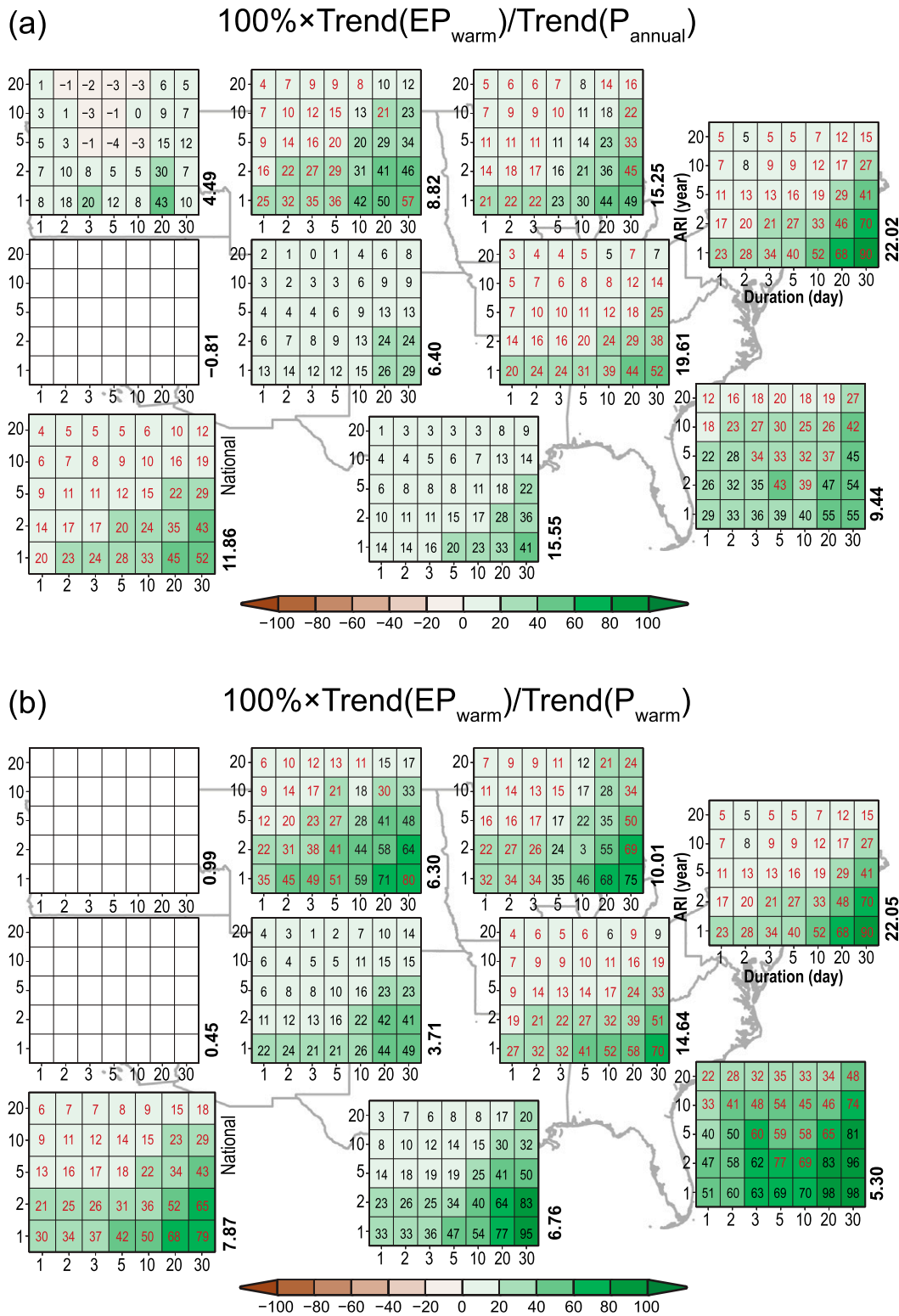


FIG. 9. As in Fig. 8, but for the warm season for the ratios (a) $T(EP_{\text{warm}}) / T(P_{\text{annual}})$ and (b) $T(EP_{\text{warm}}) / T(P_{\text{warm}})$. The rotated numbers to the right of each table are the values $[\text{mm} (10 \text{ yr})^{-1}]$ of $T(P_{\text{annual}})$ in (a) and $T(P_{\text{warm}})$ in (b). Blank regional tables represent near-zero values of $T(P_{\text{annual}})$ or $T(P_{\text{warm}})$.

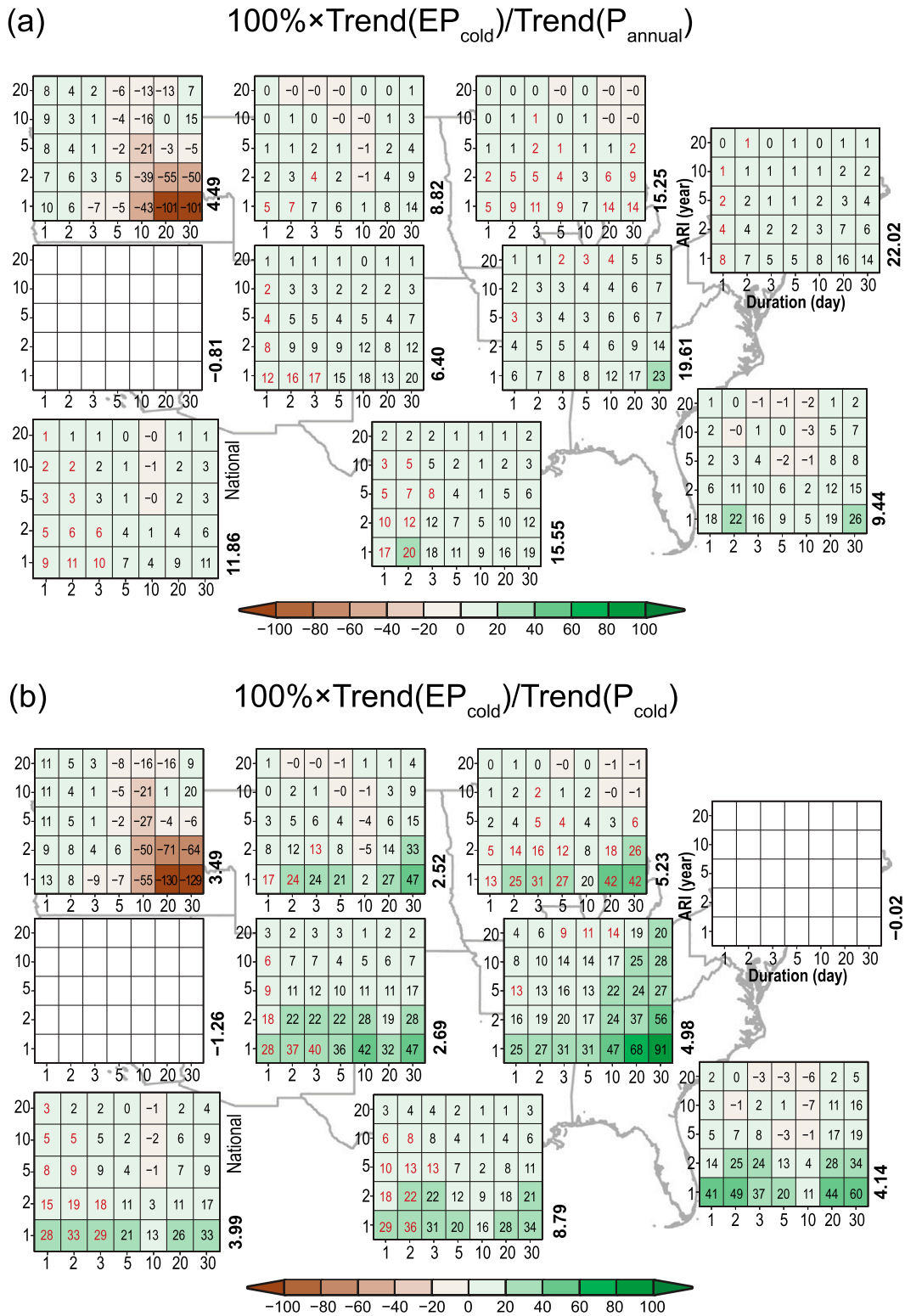


FIG. 10. As in Fig. 9, but for the cold season.

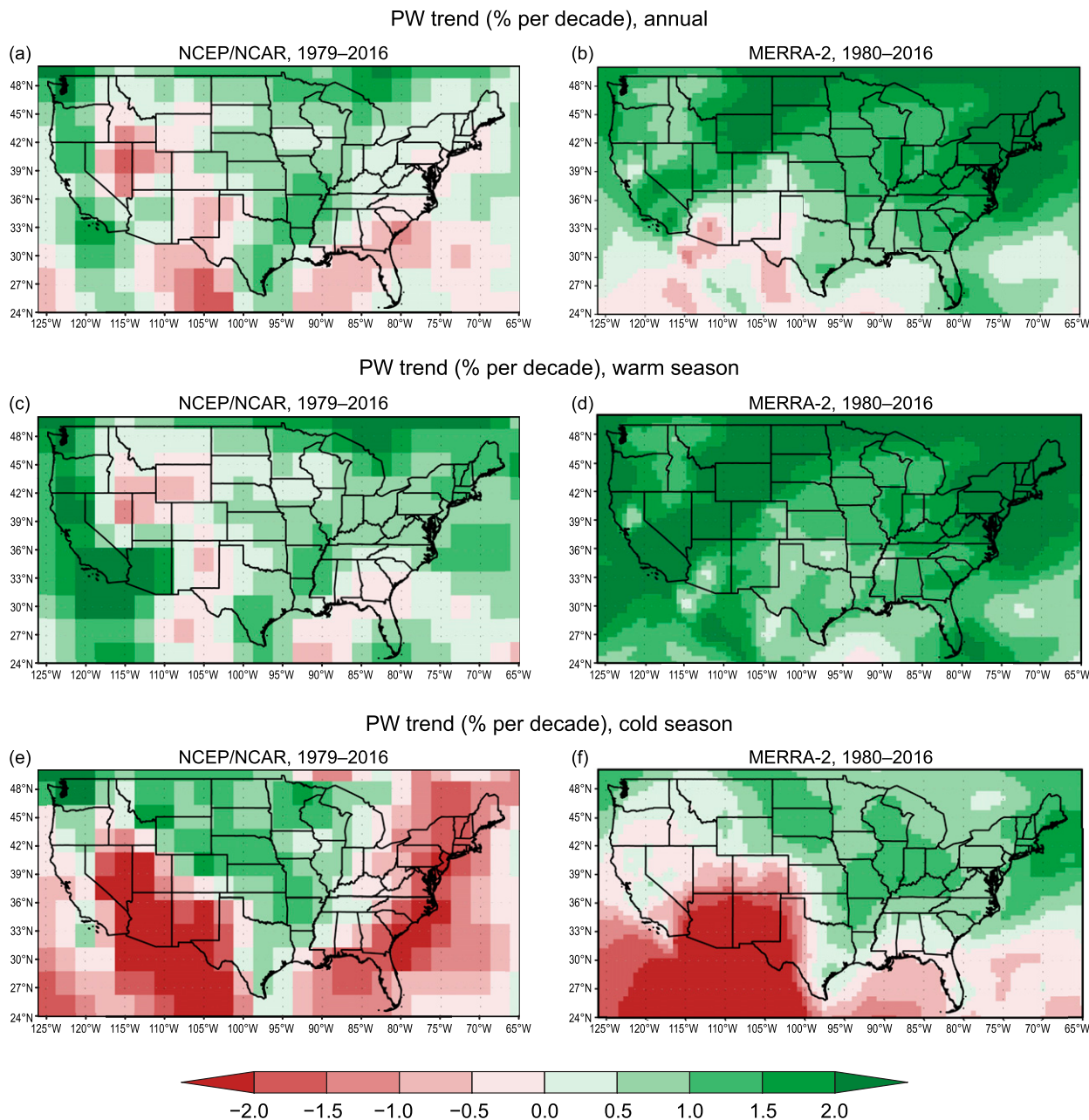


FIG. 11. Least squares trends in water vapor in percent per decade from the (left) NCEP–NCAR and (right) MERRA-2 reanalyses for (a),(b) annual, (c),(d) the warm season, and (e),(f) the cold season.

from a climatological perspective that extratropical cyclones (particularly those associated with fronts) and tropical cyclones are key factors related to extreme precipitation events with varying degrees of impact in the warm and cold seasons. Their analysis examined the same nine regions of the United States used here and an ARI of 1 in 5 years for extreme precipitation but focused on trends during the years 1895–2009, confounding any direct comparison with

the trends identified in this analysis. Nonetheless, [Kunkel et al. \(2012\)](#) identified statistically significant trends of weather types associated with extreme precipitation that vary with region and season. This suggests that a more comprehensive accounting of changes in extreme precipitation events will require knowledge of both changes in PW as well as changes in the intensity, speed, and frequency of weather types by season and region.

TABLE 2. Correlation coefficients ($\times 100$) of $T(PW)$ and $T(EP)$ across all nine regions and the warm and cold season for all combinations of ARI and duration (1–30 days). All correlations are statistically significant at the 0.01 significance level.

ARI (yr)	1 day	2 days	3 days	5 days	10 days	20 days	30 days
20	64	59	55	52	45	46	51
10	66	61	58	54	52	43	47
5	64	62	59	55	51	44	47
2	63	61	58	55	48	46	48
1	62	58	55	52	48	47	49

4. Conclusions

There are several insights that can be drawn from this analysis. Nationally, trends are upward for all 35 combinations of 1-day to 1-month durations and 1–20-yr ARIs for both the frequency of extreme events and the proportion of total precipitation contributed by the extreme events. There is relatively smaller variability with event duration in contrast to ARIs. This is especially evident for the trends of extreme precipitation frequency, but it is also evident for the proportion of total precipitation attributed to the extreme events. The trends for the frequency of extreme events are largest for ARIs of 20 years, the rarest event considered here. They are about double the trends for the small ARI value, for example, 1 year. This makes it difficult to generalize the magnitude of the trends of very rare events given trends of less rare events. This has important implications for long ARI design values derived from stationary and even nonstationary statistics when based on historically observed extreme events. ARIs beyond 20 years were not analyzed here because of insufficient sample size to assess robust regional trends, but since the trends of extreme precipitation events increased as ARIs increased, trends of extreme events with ARIs beyond 20 years may be even stronger.

There is considerable spatial and temporal variability of the extreme precipitation trends and they can vary with the chosen extreme precipitation ARI and duration. This occurs for both the trends in the frequency of extreme precipitation events as well as the proportion of total precipitation accounted for by the extreme events. Moving from the West Coast to the East Coast, there is a pattern of increasing trends in both the extremes and total precipitation, but the former is amplified by comparison. The largest positive trends of the extremes were found in the NE, ENC, and C regions with virtually all trends statistically significant. By contrast, the NW region has slightly over one-half of its trends negative and a few statistically significant. Without seasonal decomposition, for every region the 1-, 2-, and 3-day durations for 1-yr

ARIs are increasing, and, despite their short duration, these events contribute to one-third of the trend in total precipitation. This result implies that understanding the causes of short-duration extreme precipitation trends is important if total precipitation trends are to be fully explained. Similarly, for 30-day duration events, on average $\sim 60\%$ of the total precipitation trend is attributable to the wettest 30 days of the year with as much as $\sim 100\%$ in the NE.

From a seasonal perspective, the warm season has larger and more significant trends of extreme events. It is the time of the year with the largest and most significant trends of both extreme-event frequency and the proportion of total precipitation attributed to extreme events. This occurs even in areas where the cold- and warm-season precipitation are nearly equal. This highlights the importance of seasonally decomposing trends. It is also noteworthy that the warm season is the time of year with the highest values of PW, the largest upward trends and the most spatially coherent increases in PW. PW clearly plays a key role in the amount of precipitation observed in the upper tail of the precipitation distribution.

The cumulative causes of the upward trends in extreme precipitation in the United States are becoming clearer. On a global scale, it has been concluded that the upward trends in precipitation extremes are strongly affected by a warmer world through increases in water vapor (or PW) (IPCC 2013) and various other atmospheric factors (Kitoh and Endo 2016; Nie et al. 2018). Observational results here show that the trends of PW are an important seasonal and regional factor contributing to the observed change in extreme precipitation events. Other factors operating in the United States outlined by Kunkel et al. (2012) point the way to further trend analysis to better understand of the causes of the increase in extreme precipitation events, namely, frontal activity and extratropical and tropical cyclones. Because of the systematic decrease in the positive correlation of the trends of PW with extreme events for longer durations it will be important to examine the trends of the persistence as well as the intensity and frequency of extreme-event synoptic weather types at the regional level. In addition, atmospheric and oceanic teleconnections can also be relevant, for example, forcing by sea surface temperatures (Hoerling et al. 2016). As global temperatures rise, PW will increase in many regions per Clausius–Clapeyron (Kunkel et al. 2013). How this additional water vapor manifests itself seasonally, regionally, and within important synoptic weather and climate events (e.g., frontal, extratropical and tropical storms) will need to be comprehensively evaluated, both in terms of storm dynamics and thermodynamics.

The results of this work provide evidence that structures designed using precipitation statistics for a stationary climate are at risk of underdesign, especially for the most extreme rainfall rates examined here (1 in 20 years). The extreme precipitation design values that are commonly in use today, such as those provided in the NOAA Atlas 14 series (e.g., Bonnin et al. 2004), are based on the assumption of a stationary climate. Recognizing that many of those design values extend well beyond the 20-yr ARI used here, to the extent that sizable upward trends of the ARIs were found to increase as the ARIs became larger, peaking at the largest ARI analyzed, there is cause for concern. As PW increases with a warming climate, users of the NOAA Atlas 14 series would be well served by explicitly incorporating nonstationarity in future Atlas updates.

Acknowledgments. Support for this project was provided by the Strategic Environmental Research and Development Program Contract W912HQ 15-C-0010.

REFERENCES

- American Society of Civil Engineers, 2016: Failure to act: Closing the infrastructure investment gap for America's economic future. ASCE Rep., 32 pp., <https://www.infrastructurereportcard.org/wp-content/uploads/2016/10/ASCE-Failure-to-Act-2016-FINAL.pdf>.
- Ashley, S. T., and W. S. Ashley, 2008: Flood fatalities in the United States. *J. Appl. Meteor. Climatol.*, **47**, 805–818, <https://doi.org/10.1175/2007JAMC1611.1>.
- Bao, J., S. C. Sherwood, M. Colin, and V. Dixit, 2017: The robust relationship between extreme precipitation and convective organization in idealized numeral modeling simulations. *J. Adv. Model. Earth Syst.*, **9**, 2291–2303, <https://doi.org/10.1002/2017MS001125>.
- Bonnin, G. M., D. Martin, B. Lin, T. Parzybok, M. Yekta, and D. Riley, 2004: Semiarid Southwest (Arizona, Southeast California, Nevada, New Mexico, Utah). Precipitation-frequency atlas of the United States, Vol. 1, version 5.0, NOAA Atlas 14, 271 pp., https://www.nws.noaa.gov/oh/hdsc/PF_documents/Atlas14_Volume1.pdf.
- Changnon, S. A., 2006: *Railroads and Weather: From Fogs to Floods and Heat to Hurricanes, the Impacts of Weather and Climate on American Railroad*. Amer. Meteor. Soc., 136 pp.
- Doocy, S., A. Daniels, S. Murray, and T. D. Kirsch, 2013: The human impact of floods: A historical review of events 1980–2009 and systematic literature review. *PLOS Curr. Disasters*, **1**, <https://doi.org/10.1371/currents.dis.f4deb457904936b07c09daa98ee8171a>.
- Durre, I., M. J. Menne, and R. S. Vose, 2008: Strategies for evaluating quality assurance procedures. *J. Appl. Meteor. Climatol.*, **47**, 1785–1791, <https://doi.org/10.1175/2007JAMC1706.1>.
- , —, B. E. Gleason, T. G. Houston, and R. S. Vose, 2010: Robust automated quality control of daily surface observations. *J. Appl. Meteor. Climatol.*, **49**, 1615–1633, <https://doi.org/10.1175/2010JAMC2375.1>.
- Gelaro, R., and Coauthors, 2017: The Modern-Era Retrospective Analysis for Research and Applications, version 2 (MERRA-2). *J. Climate*, **30**, 5419–5454, <https://doi.org/10.1175/JCLI-D-16-0758.1>.
- Giorgi, F., F. Raffaele, and E. Coppola, 2019: The response of precipitation characteristics to global warming from climate projections. *Earth Syst. Dyn.*, **10**, 73–89, <https://doi.org/10.5194/esd-10-73-2019>.
- Groisman, P. Ya., R. W. Knight, D. R. Easterling, T. R. Karl, G. C. Hegerl, and V. N. Razuvayev, 2005: Trends in intense precipitation in the climate record. *J. Climate*, **18**, 1326–1350, <https://doi.org/10.1175/JCLI3339.1>.
- Hoerling, M., J. Eischeid, J. Perlwitz, X. Quan, K. Wolter, and L. Cheng, 2016: Characterizing recent trends in U.S. heavy precipitation. *J. Climate*, **29**, 2313–2332, <https://doi.org/10.1175/JCLI-D-15-0441.1>.
- Hollander, M., and D. A. Wolfe, 1973: *Nonparametric Statistical Methods*. John Wiley and Sons, 503 pp.
- IPCC, 2013: *Climate Change 2013: The Physical Science Basis*. T. F. Stocker et al., Eds., Cambridge University Press, 1535 pp., <https://doi.org/10.1017/CBO9781107415324>.
- Kalnay, E., and Coauthors, 1996: The NCEP/NCAR 40-Year Reanalysis Project. *Bull. Amer. Meteor. Soc.*, **77**, 437–471, [https://doi.org/10.1175/1520-0477\(1996\)077<0437:TNYRP>2.0.CO;2](https://doi.org/10.1175/1520-0477(1996)077<0437:TNYRP>2.0.CO;2).
- Karl, T. R., and A. J. Koscielny, 1982: Drought in the United States: 1894–1981. *Int. J. Climatol.*, **2**, 313–329, <https://doi.org/10.1002/joc.3370020402>.
- , and W. J. Koss, 1984: Regional and national monthly, seasonal, and annual temperature weighted by area, 1895–1983. National Climatic Data Center Historical Climatology Series 4-3, 38 pp.
- , and R. W. Knight, 1998: Secular trends of amount frequency, and intensity of precipitation across the United States. *Bull. Amer. Meteor. Soc.*, **79**, 231–241, [https://doi.org/10.1175/1520-0477\(1998\)079<0231:STOPAF>2.0.CO;2](https://doi.org/10.1175/1520-0477(1998)079<0231:STOPAF>2.0.CO;2).
- Kitoh, A., and H. Endo, 2016: Changes in precipitation extremes projected by a 20-km mesh global atmospheric model. *Wea. Climate Extremes*, **11**, 41–52, <https://doi.org/10.1016/j.wace.2015.09.001>.
- Kunkel, K. E. and R. M. Frankson, 2015: Global land surface extremes of precipitation: Data limitations and trends. *J. Extreme Events*, **2**, 1550004, <https://doi.org/10.1142/S2345737615500049>.
- , and S. M. Champion, 2019: An assessment of rainfall from Hurricanes Harvey and Florence relative to other extremely wet storms in the United States. *Geophys. Res. Lett.*, <https://doi.org/10.1029/2019GL085034>, in press.
- , and Coauthors, 1998: An expanded digital daily database for climatic resources applications in the Midwestern United States. *Bull. Amer. Meteor. Soc.*, **79**, 1357–1366, [https://doi.org/10.1175/1520-0477\(1998\)079<1357:AEDDDF>2.0.CO;2](https://doi.org/10.1175/1520-0477(1998)079<1357:AEDDDF>2.0.CO;2).
- , D. R. Easterling, D. A. Kristovich, B. Gleason, L. Stoeker, and R. Smith, 2012: Meteorological causes of the secular variations in observed extreme precipitation events for the conterminous United States. *J. Hydrometeorol.*, **13**, 1131–1141, <https://doi.org/10.1175/JHM-D-11-0108.1>.
- , T. R. Karl, D. R. Easterling, K. Redmond, J. Young, X. Yin, and P. Hennon, 2013: Probable maximum precipitation (PMP) and climate change. *Geophys. Res. Lett.*, **40**, 1402–1408, <https://doi.org/10.1002/grl.50334>.
- Melillo, J. M., T. C. Richmond, and G. W. Yohe, Eds., 2014: *Climate Change Impacts in the United States: The Third National Climate Assessment*. U.S. Global Change Research Program, 148 pp., <https://doi.org/10.7930/J0Z31WJ2>.
- Menne, M. J., I. Durre, R. S. Vose, B. E. Gleason, and T. G. Houston, 2012: An overview of the Global Historical Climatology

- Network-Daily database. *J. Atmos. Oceanic Technol.*, **29**, 897–910, <https://doi.org/10.1175/JTECH-D-11-00103.1>.
- Nie, J., A. H. Sibel, D. A. Shaevitz, and S. Wang, 2018: Dynamic amplification of extreme precipitation sensitivity. *Proc. Natl. Acad. Sci. USA*, **115**, 9467–9472, <https://doi.org/10.1073/pnas.1800357115>.
- NOAA, 2017: U.S. billion-dollar weather and climate disasters. NCEI, <https://www.ncdc.noaa.gov/billions/summary-stats>.
- O’Gorman, P., and T. Schneider, 2009: The physical basis for increases in precipitation extremes in simulation of 21st-century climate change. *Proc. Natl. Acad. Sci. USA*, **106**, 14 773–14 777, <https://doi.org/10.1073/pnas.0907610106>.
- Seager, R., A. Hooks, A. P. Williams, B. Cook, J. Nakamura, and N. Henderson, 2015: Climatological variability and trends in the U.S. vapor pressure deficit, an important fire weather quantity. *J. Appl. Meteor. Climatol.*, **51**, 1121–114, <https://doi.org/10.1175/JAMC-D-14-0321.1>.
- Soil and Water Conservation Society, 2003: Conservation implications of climate change: Soil erosion and runoff from cropland. SWCS Rep., 24 pp., https://www.swcs.org/static/media/cms/Climate_changefinal_112904154622.pdf.
- Thackeray, C. W., A. M. DeAngelis, A. Hall, D. L. Swain, and X. Qu, 2018: On the connection between hydrologic sensitivity and regional wet extremes. *Geophys. Res. Lett.*, **45**, 11 343–11 351, <https://doi.org/10.1029/2018GL079698>.
- Trenberth, K. E., J. Fasullo, and L. Smith, 2005: Trends and variability in column-integrated atmospheric water vapor. *Climate Dyn.*, **24**, 741–758, <https://doi.org/10.1007/s00382-005-0017-4>.
- Walsh, J., and Coauthors, 2014: Our changing climate. *Climate Change Impacts in the United States: The Third National Climate Assessment*, J. M. Melillo, T. C. Richmond, and G. W. Yohe, Eds., U.S. Global Change Research Program, 19–67, <https://doi.org/10.7930/J0KW5CXT>.
- Wang, J., and L. Zhang, 2008: Systematic errors in global radiosonde precipitable water data from comparisons with ground-based GPS measurements. *J. Climate*, **21**, 2218–2238, <https://doi.org/10.1175/2007JCLI1944.1>.
- Wilks, D. S., 2006: *Statistical Methods in the Atmospheric Sciences*. Elsevier, 627 pp.
- Wuebbles, D. J., D. W. Fahey, K. A. Hibbard, D. J. Dokken, B. C. Stewart, and T. K. Maycock, Eds., 2017: *Climate Science Special Report: Fourth National Climate Assessment*. Vol. 1, U.S. Global Change Research Program, 470 pp., https://science2017.globalchange.gov/downloads/CSSR2017_FullReport.pdf.